Influence of zirconium phosphate on the properties of $(VO)_2P_2O_7$ catalysts for the selective oxidation of n-butane to maleic anhydride

Sabine Zeyß,[a] Gerhard Wendt,[a]* Karl-Heinz Hallmeier,[b] Rüdiger Szargan[b] and Gerd Lippold[c]

[a] Universität Leipzig, Fakultät für Chemie und Mineralogie, Institut für Technische Chemie

[b] Institut für Physikalische und Theoretische Chemie

[c] Fakultät für Physik und Geowissenschaften, Institut für Experimentalphysik II, Linnéstr. 3, D-04103 Leipzig, Germany

The effect of zirconium phosphate on the catalytic, textural and structural properties of $(VO)_2P_2O_7$ catalysts has been studied. Catalysts with different P/V and Zr/V ratios were prepared using different preparation methods and characterized by thermo-analytical and texture measurements, X-ray diffraction (XRD), potentiometric titration, FTIR, X-ray absorption [X-ray absorption near-edge structure (XANES) and extended X-ray absorption fine structure (EXAFS)] and laser Raman spectroscopy. The n-butane conversion and the maxima of maleic anhydride (MA) yield shift to lower reaction temperatures on modification of $(VO)_2P_2O_7$ with zirconium phosphate. There is no correlation between catalytic and textural properties of the modified catalysts. The zirconium phosphate modification causes a partial amorphization of the $(VO)_2P_2O_7$ catalysts and leads to an enhancement of the $VOPO_4$ microdomains (α_I-, β-$VOPO_4$ and amorphous $VOPO_4$).

$(VO)_2P_2O_7$ catalysts are widely used as industrial catalysts for the selective oxidation of n-butane to maleic anhydride (MA). Catalysts employed in several technological processes differ in the method of preparation, the conditions during the activation and the nature and amount of promoters. The effect of promoters has been examined in a series of papers.[1-3] In particular, the modification of $(VO)_2P_2O_7$ catalysts with zirconium phosphate leads to an enhancement of the catalytic activity[4-6] and to an improvement in the mechanical properties of the catalysts.[7,8] The preparation method during the modification of the precursor with the promoter component influences the catalytic activity significantly.[6] Although the effect of the promoter modification on the properties of $(VO)_2P_2O_7$ catalysts has been investigated intensively the cause of the efficiency of the promoter interaction is still a matter of discussion.

The aim of the present investigation was to utilize different preparation and characterization methods to obtain more detailed information about the influence of zirconium phosphate promoters on the catalytic, textural and structural properties of $(VO)_2P_2O_7$ catalysts.

Experimental

Preparation of the catalysts

The preparation of the precursor $VOHPO_4 \cdot 0.5H_2O$ was carried out in an organic medium.[9] V_2O_5 was suspended in a mixture of benzyl alcohol and butan-2-ol. The suspension was stirred, heated under reflux at 383 K for 1.75 h and cooled to room temperature. A solution of H_3PO_4 (85 wt.%) in butan-2-ol was added and the reaction mixture was stirred and heated under reflux at 383 K for 5 h. The reaction mixture was cooled and filtered. The precipitate was washed twice with butan-2-ol and dried at 423 K in air for 24 h. Precursors with P/V ratios of 1.0, 1.1 and 1.2 were prepared.

The modification with zirconium phosphate was carried out by precipitation deposition using two preparation methods: method A:[6] Solutions of $ZrOCl_2 \cdot 8H_2O$ in ethylene glycol and H_3PO_4 (85 wt.%) in ethylene glycol were prepared and added simultaneously to an ethylene glycol suspension of the precursor. Precursors with P/V = 1.0, 1.1 and 1.2 were modified. Method B: $Zr(OC_3H_7)_4$ (70 wt.% in propan-1-ol) and a

solution of H_3PO_4 in propan-2-ol were added together to the propan-2-ol suspension of the precursor with P/V = 1.1. The solvents were evaporated while stirring the suspension.

All precursors with Zr/V ratios of 0.05, 0.10 and 0.15 were dried at 423 K for 24 h. The samples were then pressed (25 kN cm^{-2}, 5 min) and sieved to a granular fraction of 0.1–0.315 mm. Thermal activation was carried out in reaction gas mixture (1.5 vol.% n-butane in air). The samples were heated at a heating rate of 5 K min^{-1} from room temperature to 723 K, calcined at this temperature for 24 h and then cooled in the reaction gas.

Catalytic measurements

Catalytic measurements were performed in a U-tube integral flow stainless-steel reactor with id 10 mm. An oven with salt bath was used. 3 g catalyst in a particle fraction between 0.1 and 0.315 mm mixed with 3 g corund (α-Al_2O_3) in the particle fraction of 0.2–0.3 mm was situated in the reactor. The total gas flow was 10 l h^{-1} with a gas composition of 1.5 vol.% n-butane in air. Before the reaction the *ex situ* calcined catalysts were conditioned *in situ* at 573 K for 2 h in the reaction gas mixture. The reaction products were analysed by on-line gas chromatography (HP 5890 Series II) with CH_4 as internal standard. With the combination of a Carbosieve SII (packed) column with TCD it was possible to analyse O_2, N_2, CH_4, CO_2 and H_2O. The combination of Poraplot Q (capillary column, length 25 m, id, 0.32 mm) with FID allowed the analysis of C—H-containing compounds.

Thermoanalytical measurements

Differential thermal analysis (DTA), thermogravimetric (TG) and DTG graphs were recorded with a STA 490 QMS (Netzsch). The catalyst precursors (particle size 0.1–0.315 mm) were heated from 293–1073 K with a heating rate of 10 K min^{-1} in a helium atmosphere (0.2 l min^{-1}). By coupling the thermoanalytical equipment with the mass spectrometer it was possible to analyse the volatile products which were produced.

Characterization of the catalysts

Texture measurements. The specific surface areas [S(BET)] and the pore radii distributions were estimated with an ASAP

2000 (Micromeritics) using N_2 adsorption at 77 K.

XRD. XRD patterns were obtained with a D5000 (Siemens) using Cu-Kα radiation with $\lambda = 0.154$ nm.

FTIR spectroscopy. FTIR spectra were recorded with an FTIR spectrometer system 2000 (Perkin Elmer) with DTGS-MIR detector. 2 mg of catalyst were mixed with 100 mg KBr. This was then pressed to form a self-supporting disk.

Potentiometric titration. Potentiometric titrations were carried out using the method of Niwa and Murakami.[10] The amount and the average oxidation number of vanadium were estimated in three stages: 1, Oxidation of V^{3+} and V^{4+} to V^{5+} with $KMnO_4$; 2, potentiometric titration: reduction of obtained V^{5+} to V^{4+} with $(NH_4)_2Fe(SO_4)_2 \cdot 6H_2O$; 3, potentiometric titration: reduction of V^{5+} (of a new sample solution) to V^{4+} with $(NH_4)_2Fe(SO_4)_2 \cdot 6H_2O$. The formation of V^{3+} species can be ruled out from the obtained experimental results.

XANES/EXAFS spectroscopy. XANES and EXAFS measurements at the V K edge were used to estimate the coordination number and the oxidation state of vanadium, respectively, and the average V—O bonding distance. The XANES and EXAFS spectra were recorded in transmission at the EXAFS-II station [double-crystal monochromator with Si(111) crystals] using synchrotron radiation from DORIS-III at the Hamburger Strahlungslabor HASYLAB at DESY. The energy of the electrons in the storage ring was 4.6 GeV, the current was 25–100 mA and the spectral energy resolution at the V K edge was 1 eV. The ground powder samples were held between two Kapton foils.

Laser Raman spectroscopy. Raman spectra were obtained with the XY 800 (Dilor) with CCD array detector using an Ar^+ ion laser with the emission line at $\lambda = 514.53$ nm with different laser power densities. The spectral resolution was better than 4 cm^{-1}. Two types of samples were investigated: pressed powder samples after calcination in reaction gas mixture at 723 K and the powder of the same samples in closed quartz ampoules heated under vacuum (10^{-2} Pa) at 673 K for 12 h to avoid influence of the atmosphere during the experiment.

Results and Discussion

Catalytic measurements

The main products of n-butane conversion were MA, CO and CO_2; small amounts of side products such C_2 and C_3 cracked products, n-butane dehydrogenation products (butenes and buta-1,3-diene), acetaldehyde, acetic acid, propionic acid, acrylic acid and furan, with a total selectivity of $<3\%$ were formed. The amount of the promoter present has no influence on the formation of side products.

In Fig. 1 and 2 the n-butane conversion and the MA yield are shown as a function of the reaction temperature for catalysts with different Zr/V ratios using preparation methods A and B. The n-butane conversion increases with increasing reaction temperature and is complete at temperatures above 760 K for all catalysts. The MA yield passes through a maximum. Comparison between the catalysts with respect to the P/V ratio reveals the highest n-butane conversion for catalyst with P/V = 1.0. With increasing P/V ratio the n-butane conversion decreases but the MA selectivity increases leading to an optimum in MA yield for the catalyst with P/V = 1.1. The results obtained are in accordance with the literature.[11,12] The zirconium phosphate modification causes a shift of the n-butane conversions and of the maxima of MA yields to
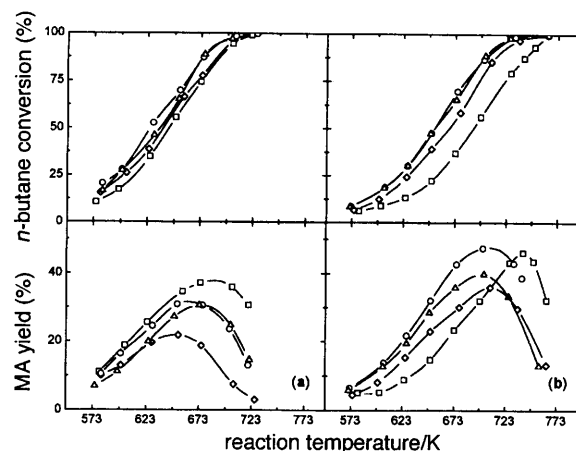
Fig. 1 Dependence of n-butane conversion and MA yield on reaction temperature for catalysts with Zr/V: □, 0; ○, 0.05; △, 0.10 and ◇, 0.15, preparation method A; $W/F_0 = 0.03$ g h l^{-1}, 1.5 vol.% n-butane in air; (a) P/V = 1.0; (b) P/V = 1.1

lower reaction temperatures. For all investigated catalysts a significant influence of the zirconium phosphate modification is observed on catalysts with Zr/V ratios between 0.05 and 0.10, with a less distinct effect for catalysts with Zr/V = 0.15. With the exception of the catalyst with P/V = 1.2 and Zr/V = 0.05 the maximal values of the MA yields decrease in comparison to the sample without zirconium phosphate (Zr/V = 0). The influence of the modification method A and B is documented in Fig. 2 for catalysts with P/V = 1.1. Precipitation deposition of the zirconium phosphate using method B leads to significantly lower MA yields in comparison with method A, due mainly to a decrease in the MA selectivity.

Thermoanalytical measurements

Fig. 3 gives a general view of the thermoanalytical investigations of precursors with P/V = 1.0 and different Zr/V ratios using preparation method A. First the DTG curves of the zirconium phosphate free sample should be discussed [Fig. 3(a)]. The peak at 385 K indicates the desorption of physically adsorbed water. The peak at 664 K is assigned to the loss of crystal water of the precursor phase $VOHPO_4 \cdot 0.5H_2O$ and that at 730 K corresponds to the water loss due to the condensation of two hydrogen phosphate groups. The mass loss is 16.6 wt.%, (after subtraction of the adsorbed water) over the whole temperature range and is higher than the value for a dehydration and dehydroxylation process (10.5 wt.%) accord-
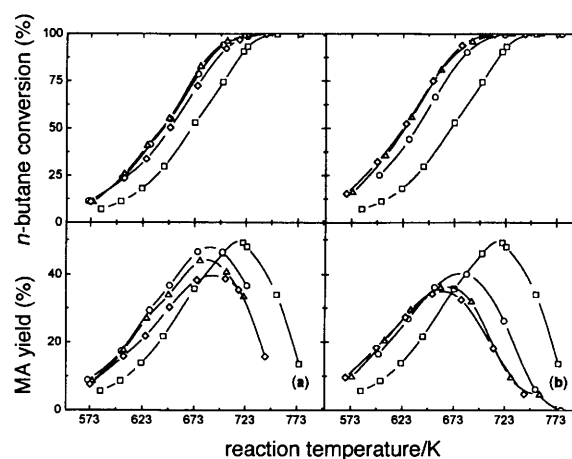
Fig. 2 Dependence of n-butane conversion and MA yield on reaction temperature for catalysts with Zr/V: □, 0; ○, 0.05; △, 0.10 and ◇, 0.15; P/V = 1.1; reaction conditions from Fig. 1; (a) preparation method A; (b) preparation method B
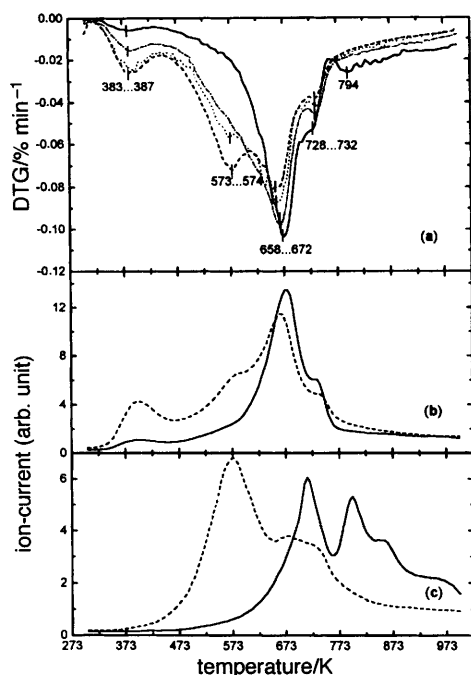
Fig. 3 Thermoanalytical investigations for precursors with P/V = 1.0 and Zr/V: (———) 0, (·······) 0.10 and (– – – –) 0.15; preparation method A; heating rate = 10 K min^{-1}: (a) DTG; (b) water loss detected by MS; (c) loss of CO_2 detected by MS

ing to eqn. (1) and (2):

$$2\,VOHPO_4 \cdot 0.5H_2O \rightarrow 2\,VOHPO_4 + H_2O \qquad (1)$$

$$2\,VOHPO_4 \rightarrow (VO)_2P_2O_7 + H_2O \qquad (2)$$
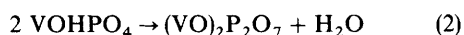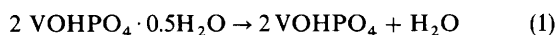
It was found by mass spectrometry that the dehydration of the sample coincides with the removal of organic species from the $(VO)_2P_2O_7$ lattice in the form of CO_2 [Fig. 3(b) and (c)]. During the preparation process some of the alcohol can be trapped between the layers of $VOHPO_4 \cdot 0.5H_2O$ and stabilized as phosphoric ester.[13] The peaks at higher temperatures (>770 K) were assigned to the removal of organic species from the lattice of the precursor exclusively. This result is in agreement with that of Cavani et al.[13] Furthermore, in the temperature range 573 to 893 K the release of small amounts of benzyl alcohol could be detected by mass spectroscopy (tropylium ion with m/z 91).

The zirconium phosphate modification using preparation method A leads to a significant change in the thermal behaviour of the precursors. First, a new DTG peak at 574 K appears and, second, the peak at 672 K is shifted to lower temperatures [658 K, Fig. 3(a)]. It can be recognized that the main peak of the zirconium phosphate modified samples at 658 K corresponds to a loss of water and removal of organic species [Fig. 3(b) and (c)]. The DTG peak at 574 K corresponds to both the dehydration and the removal of organic species from the framework. The dehydration step can be attributed to the transformation of $Zr(HPO_4)_2 \cdot H_2O$ to ZrP_2O_7.[14] In contrast to the zirconium phosphate-free sample the dehydration and removal of organic species is complete at temperatures >830 K.

The results of the thermoanalytical investigations of zirconium phosphate modified precursors with P/V = 1.1 and 1.2 using preparation method A are comparable to those obtained with P/V = 1.0.

A significant difference in the thermal behaviour of the precursors was found between the preparation methods A and B. It was established that the DTG curves of zirconium phosphate modified samples prepared by method B are not distinguished significantly from the DTG curve of the $VOHPO_4 \cdot 0.5H_2O$ precursor. The dehydration is also super-

imposed by the removal of organic species. Only the mass loss enhances with increasing Zr/V ratio owing to the zirconium phosphate transformation.

Characterization of the catalysts

Texture measurements. In Table 1 the specific surface areas are summarized for catalysts with different P/V and Zr/V ratios. The values obtained are expected for $(VO)_2P_2O_7$ catalysts prepared in an organic medium.[15] The specific surface areas do not reveal large variations and do not depend significantly on the preparation method and amount of zirconium phosphate. The pore analysis data showed that the samples contain only meso- and macro-pores with pore diameters predominantly in the range 10–25 nm. Therefore, it is concluded that the zirconium phosphate influence on the catalytic activity and selectivity cannot be attributed to textural effects.

XRD. XRD analysis of the precursor samples exhibits only the XRD patterns for the $VOHPO_4 \cdot 0.5H_2O$ phase.[16] Calcination at 723 K in the reaction gas mixture leads to the formation of $(VO)_2P_2O_7$. The XRD patterns of the catalyst with P/V = 1.0 modified with zirconium phosphate using method A are shown in Fig. 4. In comparison with the $(VO)_2P_2O_7$ sample (Zr/V = 0) zirconium phosphate modification does not give rise to a shift in the reflection position in all investigated samples. This was also found on samples prepared using method A or B with different P/V ratios. Therefore incorporation of the zirconium component in the $(VO)_2P_2O_7$ lattice affording $[\{(VO)_{1-x}M_x\}_2P_2O_7]^2$ can be ruled out. However, with increasing Zr/V ratio a decrease in the peak intensity and an increase in the background are observed. It can be concluded that modification with zirconium phosphate causes a partial amorphization of the investigated $(VO)_2P_2O_7$ catalysts. In the diffraction pattern of the sample with Zr/V = 0.05 a small additional reflection at d = 0.412 nm (2θ = 21.5°) is detected and is assigned to the most intense (200) reflection of the ZrP_2O_7 phase. At higher zirconium phosphate contents the peak cannot be identified because of broadening of the (200) reflection of the $(VO)_2P_2O_7$ phase and increasing background.

In a series of publications it was shown that the n-butane conversion is a structure sensitive reaction with respect to the special action of the (200) plane of the catalytically active $(VO)_2P_2O_7$ phase.[17–20] In this connection, the intensity ratio $I(200)/[I(200) + I(042) + I(202) + I(063)]$ using the integral intensities (peak areas) was calculated. The exact estimation requires a very small step width (2θ = 0.025°) during the XRD measurements. The results obtained are summarized in Table 2. With increasing Zr/V ratio a formal enhancement of the intensity ratio $I(200)/[I(200) + I(042) + I(202) + I(063)]$ is recognizable. Considering the overlapping of the (200) reflection of the $(VO)_2P_2O_7$ phase with that of the ZrP_2O_7 phase and the higher amorphization of the modified samples there is no definite indication of the influence of the zirconium phosphate modification on the exposure of the (200) plane of the $(VO)_2P_2O_7$ phase.

Table 1 Specific surface area (BET) in m^2 g^{-1} of the catalysts with different P/V and Zr/V ratios, calcined at 723 K for 24 h in 1.5 vol.% n-butane in air

	P/V ratio			
	method A $ZrOCl_2 \cdot 8H_2O$			method B $Zr(OC_3H_7)_4$
Zr/V ratio	1.0	1.1	1.2	1.1
0	29	29	22	29
0.05	25	25	23	28
0.10	27	23	25	30
0.15	24	25	20	30
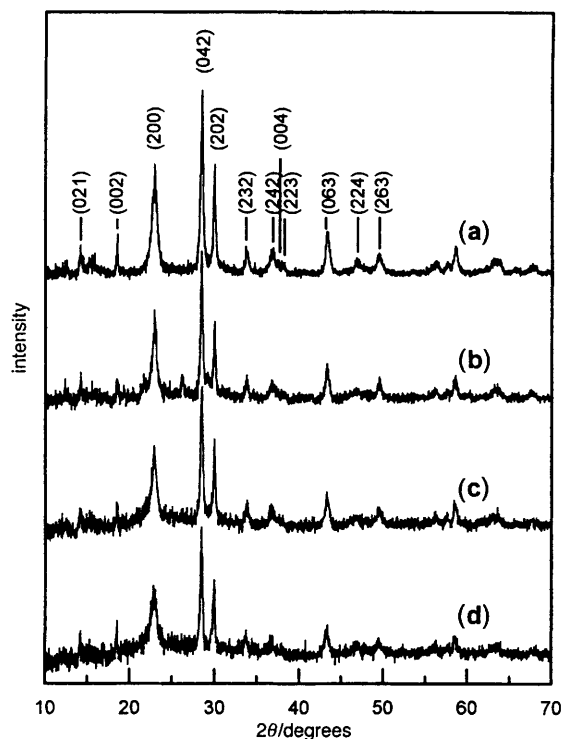
Fig. 4 XRD patterns of catalysts with P/V = 1.0 and Zr/V: (a) 0, (b) 0.05, (c) 0.10 and (d) 0.15; preparation method A

Fig. 5 FTIR spectra of catalysts with P/V = 1.0 and Zr/V: (a) 0, (b) 0.05, (c) 0.10 and (d) 0.15; preparation method A

FTIR spectroscopy. Similar information about the phase composition was obtained using FTIR spectroscopy. The FTIR spectra of the calcined $(VO)_2P_2O_7$ with P/V = 1.0 modified with zirconium phosphate are shown in Fig. 5. The spectra obtained are characteristic of $(VO)_2P_2O_7$ samples. The mode assignment was carried out corresponding to literature data[21-26] and is summarized in Table 3. The position of the $(VO)_2P_2O_7$ modes does not change on modification with zirconium phosphate. Thus there is no indication for substitution of vanadium by zirconium in the lattice of $(VO)_2P_2O_7$. With increasing zirconium phosphate content an enhancement of the spectra background was observed. In accordance with the XRD data this finding is explained by amorphization of the modified $(VO)_2P_2O_7$ samples.

Determination of the average vanadium oxidation state. The average vanadium oxidation states estimated by potentiometric titration are listed in Table 4 for catalysts with different P/V and Zr/V ratios. The values for the non-modified as well as for the zirconium phosphate-containing $(VO)_2P_2O_7$ catalysts decrease with increasing P/V ratio. The existence of catalytically active V^{5+} sites depending on the P/V ratio of $(VO)_2P_2O_7$ catalysts was reported by several authors.[11,12,27]

Catalysts with a small deficiency of phosphorus (P/V $\leqslant$ 1.0) are more sensitive to oxidation than catalysts with a small excess of phophorus (P/V $\geqslant$ 1.0). Considering the dependence on the Zr/V ratio (for constant P/V ratio) it is evident that modification of the catalysts with zirconium phosphate leads to an increase in average vanadium oxidation state. The influence is lower for catalysts with higher P/V ratio. The highest amounts of V^{5+} sites were found for catalysts with Zr/

Table 3 Assignment of FTIR modes for $(VO)_2P_2O_7$ catalysts modified with zirconium phosphate

wavenumber cm^{-1}	assignment
1244	
1220	
1143	$\nu_{as}(PO_3)$
1117	
1088	
1010	$\nu_s(PO_3)$
974	$\nu(V=O)$
921	$\nu_{as}(P-O-P)$
794	$\nu[V-(O=V)]$
744	$\nu_s(P-O-P)$
634	$\delta_{as}(PO_3)$
577	
513	$\delta_s(PO_3)$
427	

Table 2 Intensity ratio $I(200)/[I(200) + I(042) + I(202) + I(063)]$ of the most intense reflections in XRD pattern of catalysts with different P/V and Zr/V ratios

	P/V ratio			
	method A ZrOCl$_2 \cdot$ 8H$_2$O			method B Zr(OC$_3$H$_7$)$_4$
Zr/V ratio	1.0	1.1	1.2	1.1
0	0.398	0.424	0.394	0.424
0.05	0.399	0.425	0.400	0.432
0.10	0.411	0.439	0.404	0.430
0.15	0.449	0.474	0.434	0.447

Table 4 Average oxidation number of vanadium in catalysts with different P/V and Zr/V ratios

	P/V ratio			
	method A ZrOCl$_2 \cdot$ 8H$_2$O			method B Zr(OC$_3$H$_7$)$_4$
Zr/V ratio	1.0	1.1	1.2	1.1
0	4.065	4.051	4.035	4.051
0.05	4.193	4.099	4.038	4.101
0.10	4.148	4.043	4.049	4.143
0.15	4.090	4.040	4.032	4.116

Zr/V = 0.05 and 0.10, independent of the preparation method. With respect to the XRD measurements it is suggested that, in the activation process from the precursor to the catalyst, zirconium phosphate influences the crystallization of the $(VO)_2P_2O_7$ phase. The partial amorphization promotes the overoxidation and hence the formation of $VOPO_4$ phases. Different results were obtained using preparation method A and B comparing catalysts with constant P/V and Zr/V ratio (Table 4). The lower values in the case of method A ($ZrOCl_2 \cdot 8H_2O$ as zirconium component) can be explained by the presence of small amounts of HCl as reducing agent formed in the activation process.

XANES/EXAFS spectroscopy.

The measured spectra were background corrected, subtracting the extrapolated contribution μ_B from the pre-edge region from the experimental data using a second-order polynomial function and were normalized at 5590 eV. The energy scale was calibrated using the pre-edge absorption peak of the standard sample V_2O_5 at 5469 eV.[28] With the definition of the edge energy at the inflection point of the main absorption edge conversion of the energy range in the k-range was carried out. $\mu_0(k)$ as an expression for the atomic absorption was obtained by a fourth-order polynomial fit. A k^3-weighted Fourier transformation was carried out using a BESSEL window for the transformation to the R space. In the case of the calcined sample with Zr/V = 0.15 a k^2-weighted Fourier transformation was used owing to the lower statistics of the measured curve. After this Fourier transformation it was possible to obtain the contribution of the several coordination spheres surrounding the absorber atom in R space.

XANES.

Fig. 6 shows the V K XANES spectra of the calcined catalysts with P/V = 1.0 and different Zr/V ratios (preparation method A) and of V_2O_5. The XANES spectra show the expected typical shape for K absorption spectra of transition metals with partially filled d orbitals. All spectra exhibit a pre-edge absorption structure which is attributed to the 1s → 3d transition. This transition is dipole forbidden in the atomic case. Nevertheless this transition can occur if the coordination geometry of the absorber atom does not have an inversion center or if lattice disorder around the absorber atom appears. Some dipole character of the transition arises by d–p mixture. Thus the intensity of the pre-edge absorption structure gives information about the local geometry around

the absorber atom. The energy position of the pre-edge absorption structure can be correlated with the electronegativity of the ligands and the coordination number. From these results, information about the oxidation state of the absorber atom can be derived. The main absorption structure originates from 1s → 4p transitions. Furthermore, the coordination geometry influences the multiple scattering processes in the XANES region.[29] The pre-edge absorption peaks have energy values of ca. 5468 eV (Fig. 6). A shift to higher energy values was noted on zirconium phosphate modification. The greatest effect was established for the catalyst with the lowest Zr/V ratio of 0.05. A change in the coordination number of vanadium in zirconium phosphate modified samples is improbable because neither a shift of the position of the reflections or modes nor new reflections in the diffraction pattern or new modes in the FTIR spectra, respectively, were observed on changing the Zr/V ratio of the samples. Considering the results of XRD and FTIR measurements and that of potentiometric titration, an increase in the energy values of the pre-edge absorption peak is due to an enhancement in the average oxidation number of vanadium. In the case of the same atoms surrounding the vanadium in the first coordination sphere the energy shift of the pre-edge absorption peak amounts to 1 eV between spectra of V^{4+} and V^{5+}.[30] A similar tendency is indicated in the V K XANES spectra of the precursor.[31]

EXAFS.

Fig. 7 shows the moduli of the Fourier transformation of V K EXAFS spectra of the calcined samples with P/V = 1.0 and different Zr/V ratios. From these graphs the relative average V—O bond distances can be determined. These were not phase and amplitude corrected and thus represent only relative data. It can be recognized that the zirconium phosphate modification results in a significant increase in the relative average V—O bond distance due to a greater amorphization in the zirconium phosphate modified catalysts. The greatest influence was again observed for the catalyst with Zr/V = 0.05. Hence it can be concluded that the maximal regrouping of the $(VO)_2P_2O_7$ lattice is reached for very small Zr contents. A further structure is indicated at 2.7 Å in the moduli of Fourier transformation of V K EXAFS spectra of the precursors[31] which is assigned to the relative average V—V bonding distance in analogy to the moduli of Fourier transformation of V K EXAFS spectra of V_2O_5 by Vlaic and Garbassi.[28] After calcination of the precursors with reaction gas a significant decrease in this relative part of the structure was found owing to the increasing amorphization.
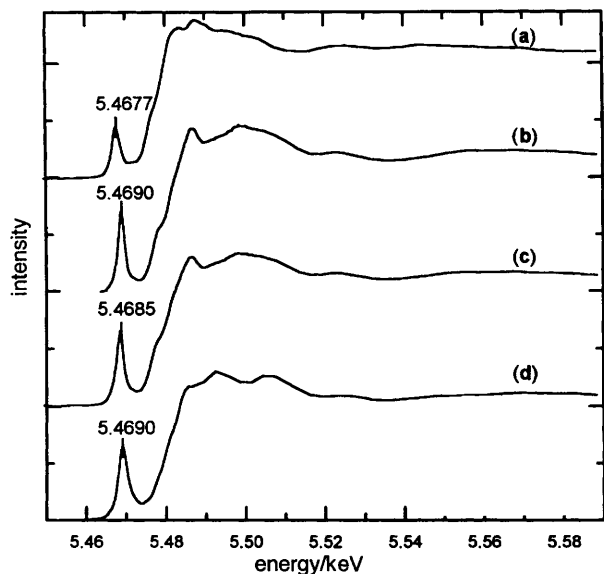
Fig. 6 V K XANES spectra of catalysts with P/V = 1.0 and Zr/V: (a) 0, (b) 0.05, and (c) 0.15, preparation method A and (d) V_2O_5
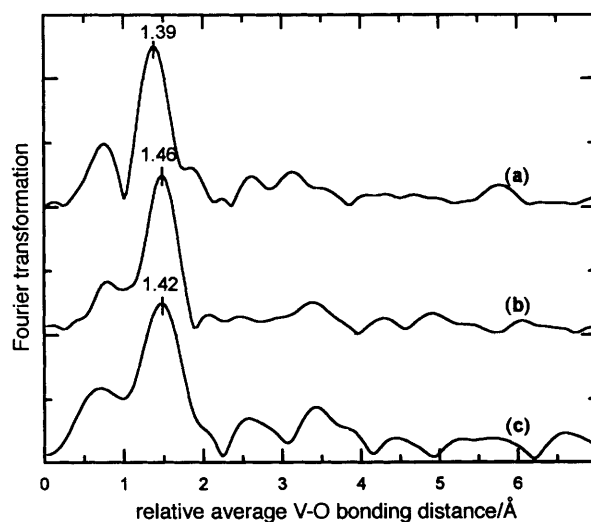
Fig. 7 Moduli of Fourier transformation of V K EXAFS spectra of catalysts with P/V = 1.0 and Zr/V: (a) 0, (b) 0.05 and (c) 0.15, preparation method A

Laser Raman spectroscopy. The laser Raman spectra were recorded to assign the $VOPO_4$ phases formed during activation in the reaction gas mixture. To be sure that no significant modification of the samples takes place on the laser application the power density dependence of the local temperature was estimated using the results of Stokes and anti-Stokes Raman measurements. Fig. 8 shows laser Raman spectra in the anti-Stokes range of $(VO)_2P_2O_7$ with P/V = 1.0 using increasing and decreasing laser power densities, respectively. The investigated sample is stable up to a power density of 400 W cm^{-2}. This result was found for measurements under vacuum and in air. The temperature, T, of the sample in the laser focus was estimated considering the intensities of the modes in the Stokes and anti-Stokes region according to:[32]

$$\frac{I_{\text{anti-Stokes}}}{I_{\text{Stokes}}} = \frac{n}{n+1} = f(T) \tag{I}$$

where n is the Bose–Einstein-factor as defined below:

$$n = \frac{1}{\exp(\hbar\Omega/kT) - 1} \tag{II}$$

where $\hbar$ is the Planck constant divided by 2π, Ω is the phonon frequency and k is the Boltzmann constant. Under our experimental conditions, the temperature (in K) in the laser focus was found to be a linear function of the laser power density p[W cm^{-2}], which can be described for the sample $(VO)_2P_2O_7$ with P/V = 1.0 by:

$$T = (304 + 1.6832 \text{ W}^{-1} \text{ cm}^2 \, p)\text{K} \tag{III}$$

(In Fig. 8 there is no linear variation of the Raman intensity with laser power density because of the temperature dependence of the anti-Stokes Raman intensity. From the lowest to the highest applied power density the temperature in the laser focus increases by *ca.* 700 K.) For further investigations of the modified $(VO)_2P_2O_7$ samples a laser power density of 12 W cm^{-2} was utilised which leads to an increase in the temperature of *ca.* 20 K according to eq. (III). It is assumed that no change in the vanadium oxidation state takes place at temperatures < 324 K.

Fig. 9 shows the laser Raman spectra of $(VO)_2P_2O_7$ catalysts with P/V = 1.0 and different Zr contents, prepared using method A. The spectra obtained are typical for $(VO)_2P_2O_7$ catalysts. According to Moser and Schrader[33] the main modes of $(VO)_2P_2O_7$ at 933 and 925 cm^{-1} can be assigned to v_{as} (P—O—P) modes. The splitting of these modes is due to two pyrophosphate groups with different P—O—P angles. Using the results of the investigation on vanadium phosphate reference substances[34] all modes, with the exception of those at
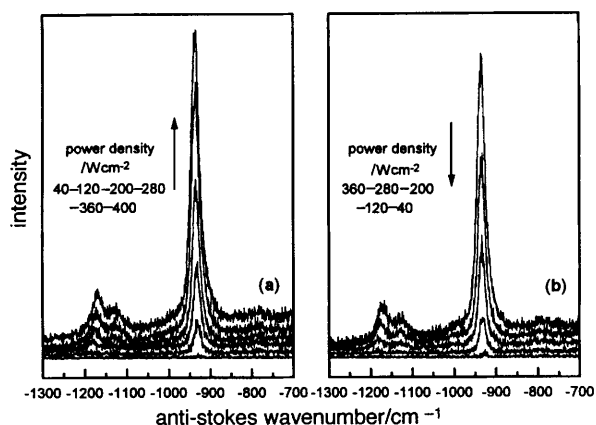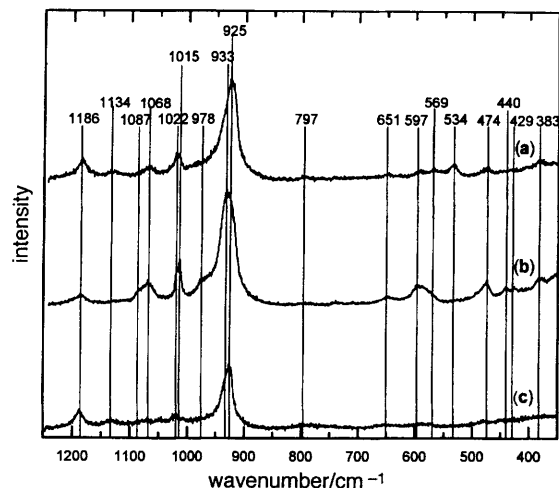
Fig. 9 Laser Raman spectra of catalysts with P/V = 1.0 and Zr/V: (a) 0, (b) 0.05 and (c) 0.15, preparation method A; measurement in air; power density = 12 W cm^{-2}

797 and 534 cm^{-1}, can be assigned to $(VO)_2P_2O_7$ modes. The modes at 797 and 534 cm^{-1} are due to the β-$VOPO_4$ and the α_I-$VOPO_4$ phase, respectively. Most of the $(VO)_2P_2O_7$ modes overlap with modes of the $VOPO_4$ phases (α_I, α_{II}, β, γ and δ). It is difficult to decide which of the $VOPO_4$ phases are formed because of the low content of $VOPO_4$ phases in the $(VO)_2P_2O_7$ lattice. Amorphous $VOPO_4$ phases cannot be ruled out and should be present in the samples. The laser Raman spectra of the zirconium phosphate modified $(VO)_2P_2O_7$ samples are nearly identical to that of unmodified $(VO)_2P_2O_7$.

Conclusions

Modification of $(VO)_2P_2O_7$ catalysts with zirconium phosphate enhances the catalytic activity for *n*-butane conversion and leads to a shift in the MA yields curves to lower temperatures, depending on the P/V ratio of the catalysts. A significant influence is observed on catalysts with low Zr/V ratios of 0.05 and 0.10. In this connection the preparation method is of importance. There is no correlation between catalytic and textural properties of the catalysts.

XRD and FTIR investigations indicate that no incorporation of the zirconium phosphate in the $(VO)_2P_2O_7$ lattice takes place. During the activation process from the precursor phase $VOHPO_4 \cdot 0.5H_2O$ to the catalytically active $(VO)_2P_2O_7$ phase an amorphous phase is formed:[1]

$$VOHPO_4 \cdot 0.5H_2O \rightarrow \text{amorphous phase} \rightarrow$$

$$(VO)_2P_2O_7 \rightarrow V^{5+}\text{-phases} \tag{3}$$
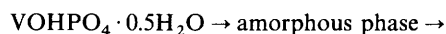
Recently published results[35] using *in situ* Raman spectroscopy revealed that, during the process of activation, the crystalline structure of $VOHPO_4 \cdot 0.5H_2O$ becomes totally disordered. The reaction products influence the final state of the catalyst with respect to the amount of the $VOPO_4$ phases.[35]

From our investigations, it is suggested that zirconium phosphate influences the transformation of the intermediate amorphous (disordered) phase into the crystalline $(VO)_2P_2O_7$ phase. As a result, a partial amorphization of the $(VO)_2P_2O_7$ phase is observed. The partial amorphization of the $(VO)_2P_2O_7$ phase by promoter component leads to higher amounts of $VOPO_4$ phases during the activation in the reaction gas mixture as shown by XANES measurements and potentiometric titration. From the laser Raman spectroscopic measurements, it is evident that small amounts of α_I- and β-$VOPO_4$ are formed. Furthermore, the presence of amorphous $VOPO_4$ phases cannot be excluded. In accordance with the

Fig. 8 Raman intensities *vs.* anti-Stokes Raman shift for $(VO)_2P_2O_7$ with P/V = 1.0 using different laser power densities; vacuum-heated sample; (a) increasing laser power density; (b) decreasing laser power density

literature it is assumed that $VOPO_4$ microdomains are formed in the $(VO)_2P_2O_7$ lattice.[36-41]

With respect to the obtained results, the effect of the zirconium phosphate modification on the catalytic properties of $(VO)_2P_2O_7$ in n-butane oxidation is connected with the formation of $VOPO_4$ phases under the influence of the reaction gas mixture. The role of V^{5+} species in the complex reaction network of n-butane oxidation is still a matter for discussion.[9] It is assumed that V^{5+} species participate in the C—H bonding abstraction of the n-butane molecule and that both oxygen insertion and total oxidation occur on V^{5+} centres.[15,42,43] High MA yields can be reached if, besides $(VO)_2P_2O_7$ small amounts of isolated V^{5+} species are present.[43] When the density of the V^{5+} centres increases, the MA selectivity decreases due to preferential total oxidation.[44] In this connection it is suggested that the $VOPO_4$ phases formed in the $(VO)_2P_2O_7$ lattice due to the zirconium phosphate modification influence significantly n-butane conversion, MA selectivity and MA yield.

References

1   F. Cavani and F. Trifirò, Stud. Surf. Sci. Catal., 1995, 91, 1.
2   G. J. Hutchings, Appl. Catal., 1991, 72, 1.
3   B. K. Hodnett, Catal. Rev.-Sci. Eng., 1985, 273, 373.
4   R. Sant and A. Varma, J. Catal., 1993, 143, 215.
5   M. T. Sananés, J. O. Petunchi and E. A. Lombardo, Catal. Today, 1992, 15, 527.
6   M. Ai, Appl. Catal., 1986, 28, 223.
7   K. Uihlein, G. Emig, J. Werther and H. Kuhne, Dechema Jahrestagung, 1992, 293.
8   G. Emig and F-G. Martin, Ind. Eng. Chem. Res., 1991, 30, 1110.
9   F. Cavani and F. Trifirò, Catalysis, Specialist Periodical Reports, The Royal Society of Chemistry, Cambridge, 1994, vol. 11, p. 246.
10 M. Niwa and Y. Murakami, J. Catal., 1982, 76, 9.
11 B. K. Hodnett, P. Permanne and B. Delmon, Appl. Catal., 1983, 6, 231.
12 B. K. Hodnett and B. Delmon, J. Catal, 1984, 88, 43.
13 F. Cavani, G. Centi, F. Trifirò and G. Poli, J. Therm. Anal., 1985, 30, 1241.
14 A. Clearfield, in Inorganic Ion Exchange Materials, ed. A. Clearfield, CRC Press, Boca Raton, FL, 1982, p. 1.
15 J. R. Ebner and M. R. Thompson, Catal. Today, 1993, 16, 51.
16 E. Bordes, Catal. Today, 1987, 1, 499.
17 G. Centi, F. Trifirò, J. R. Ebner and M. Franchetti, Chem. Rev., 1988, 88, 55.
18 I. Matsuura and M. Yamazaki, in New Developments in Selective Oxidation, ed. G. Centi and F. Trifirò, Elsevier, Amsterdam, 1990, p. 563.
19 T. Okuhara, K. Inumaru, and M. Misono, in Catalytic Selective Oxidation, ACS Symp. Ser. 523, ed. J. Hightower and T. Oyama, 1993, p. 156.
20 J. C. Volta, K. Bere, Y. J. Zhang and R. Olier, in ref. 19, p. 217.
21 E. Bordes and P. Courtine, J. Catal., 1979, 57, 236.
22 G. Busca, F. Cavani, G. Centi and F. Trifirò, J. Catal., 1986, 99, 400.
23 N. H. Batis, H. Batis, A. Ghorbel, J. C. Védrine and J. C. Volta, J. Catal., 1991, 128, 248.
24 T. P. Moser and G. L. Schrader, J. Catal., 1985, 92, 216.
25 M. López-Granados, J. C. Conesa and M. Fernández-García, J. Catal., 1993, 141, 671.
26 Z. Sobalik, S. Gonzalez and P. Ruiz, Stud. Surf. Sci., 1994, 91, 727.
27 F. Cavani, G. Centi, I. Manenti and F. Trifirò, Ind. Eng. Chem. Prod. Res. Dev., 1985, 24, 221.
28 G. Vlaic and F. Garbassi, J. Catal., 1990, 122, 312.
29 X-Ray Absorption, Principles, Applications, Techniques of EXAFS, SEXAFS and XANES, ed. D. C. Koningsberger and R. Prins, Wiley, New York, 1988, p. 573.
30 J. Wong, F. W. Lytle, R. P. Messmer and D. M. Maylotte, Phys. Rev. B, 1984, 30, 5596.
31 S. Zeyß, Dissertation, Universität Leipzig, 1995.
32 G. R. Wilkinson, in The Raman Effect, Volume 2: Applications, ed. A. Anderson, Marcel Dekker, New York, 1973, p. 811.
33 T. P. Moser and G. L. Schrader, J. Catal., 1985, 92, 216.
34 F. B. Abdelouahab, R. Olier, N. Guilhaume, F. Lefebvre and J. C. Volta, J. Catal., 1992, 134, 151.
35 G. J. Hutchings, A. Desmartin-Chomel, R. Olier and J. C. Volta, Nature (London), 1994, 368, 41.
36 M. Abon, K. E. Bere, A. Tuel and P. Delichere, J. Catal., 1995, 156, 28.
37 P. Courtine, in Solid State Chemistry in Catalysis, ACS Symp. Ser. 279, ed. R. K. Grasselli and J. F. Brazdil, 1983, 37.
38 L. Monceaux and P. Courtine, Eur. J. Solid State Inorg. Chem., 1991, t28, 233.
39 N. Harrouch Batis, H. Batis, A. Ghorbel, J. C. Védrine and J. C. Volta, J. Catal., 1991, 128, 248.
40 Y. Zhang-Lin, M. Forissier, R. P. Sneeden, J. C. Védrine and J. C. Volta, J. Catal., 1994, 145, 256.
41 Y. Zhang-Lin, M. Forissier, J. C. Védrine and J. C. Volta, J. Catal., 1994, 145, 267.
42 U. Rodemerck, Dissertation, Ruhr-Universität Bochum, 1994.
43 F. Cavani, G. Centi, F. Trifirò and R. K. Grasselli, Catal. Today, 1988, 3, 185.
44 Y. Zhang, R. P. A. Sneeden and J. C. Volta, Catal. Today, 1993, 16, 39.